DESIGN, MODELING AND ANALYSIS OF A NOVEL PIEZOACTUATED XY NANOPOSITIONER SUPPORTING BEAMLINE OPTICAL SCANNING

Lingfei Wang*, Guangcai Chang, Zongyang Yue, Lu Zhang, Shanzhi Tang
Institute of High Energy Physics, Beijing, P. R. China

Abstract

In recent years, with the advancement of X-ray optics technology, the spot size of synchrotron beamlines has been reduced to 10nm or even smaller. The reduction in spot size and the emergence of ultra-bright synchrotron sources necessitate higher stability, resolution, and faster scanning speeds for positioning systems. This paper presents the design, analysis, and simulation of an XY piezoelectric driven nanopositioning platform that supports high-precision optical scanning systems. To achieve fast and highly precise motion under the load of an optical system, a design scheme based on a hollow structure with flexible amplification and guiding mechanisms is proposed. This scheme increases displacement output while minimizing coupling displacement to ensure a high natural frequency. The rationality of this platform design is verified through modeling and finite element simulation.

INTRODUCTION

The High Energy Photon Source (HEPS) is a new generation light source that offers enhanced brightness and performance capabilities. The hard x nanoprobe beamline is primarily utilized for nanoscale scientific research. The minimum spot size can be less than 10 nm. Owing to the limitations inherent in conventional stepper motors, piezoelectric actuators have emerged as the preferred choice in this field, offering advantages such as exceptional positioning accuracy, rapid response times, compact dimensions, and lightweight construction.

The piezoelectric actuators utilized in synchrotron radiation light sources can be broadly categorized into two groups. One category encompasses the piezoelectric stick-slip actuators, which operate based on the principle of frictional inertia [1, 2]. These actuators are predominantly employed for large-scale position adjustments. One is the direct drive piezoelectric scanning platform [3–5], which is mostly used for sample scanning. This paper introduces an XY scanning platform specifically designed for nano-scanning experiments conducted at light sources. Subsequent chapters will provide detailed explanations on the structural design, static modeling, and simulation analysis of the XY scanning platform.

DESIGN OF THE MECHANICAL STRUCTURE

The schematic diagram of the nano-positioning platform driven by a piezoelectric stack is illustrated in Fig. 1. The nano-positioning platform features a symmetrical structure, comprising a bridge amplifying mechanism, two sets of guiding mechanisms, a piezoelectric stack, and a central moving stage. The piezoelectric stack is integrated into the bridge amplifying mechanism through a preload bolt, while the end of the bridge mechanism is connected to both the base and central moving stage via two sets of guiding mechanisms, ensuring optimal platform stiffness. The central moving stage adopts a hollow structure design with screw holes at the four corners, which facilitates scanning experiments and the installation of position feedback lenses.
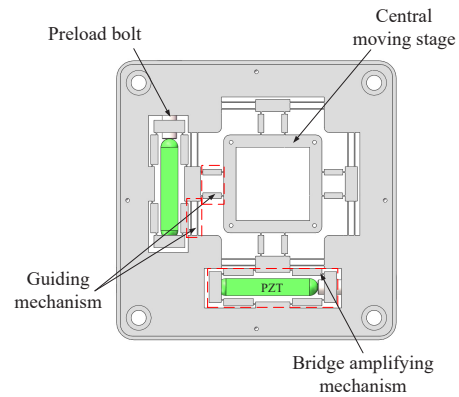
Figure 1: Schematic diagram of the XY positioning platform.

MODELING AND ANALYSIS

The amplifying mechanism analyzed in this paper is a planar mechanism, thus only the deformation of flexible hinges within the plane needs to be considered. The model diagram of the prismatic beam hinge is illustrated in Fig. 2. The thickness, width and length of the hinge are expressed by h, t_b and l_b, the loads on the prismatic beam flexure hinge are F_{xi}, F_{yi} and M_{zi}. and the flexibility matrix of the prismatic beam hinge can be obtained by considering it as a cantilever beam.

The expression of the flexibility matrix of the prismatic beam hinge [6] is as follows:

$$\begin{bmatrix} \delta x \\ \delta y \\ \delta \theta \end{bmatrix} = \begin{bmatrix} c_{11} & c_{12} & c_{13} \\ c_{21} & c_{22} & c_{23} \\ c_{31} & c_{32} & c_{33} \end{bmatrix} \begin{bmatrix} F_{xi} \\ F_{yi} \\ M_{zi} \end{bmatrix} \quad (1)$$

$$\begin{bmatrix} c_{11} & c_{12} & c_{13} \\ c_{21} & c_{22} & c_{23} \\ c_{31} & c_{32} & c_{33} \end{bmatrix} = \begin{bmatrix} \frac{l_b}{Eht_b} & 0 & 0 \\ 0 & \frac{4l_b^3}{3Eht_b^3} + \frac{l_b}{Ght_b} & \frac{6l_b^2}{Eht_b^3} \\ 0 & \frac{6l_b^2}{Eht_b^3} & \frac{12l_b}{Eht_b^3} \end{bmatrix} \quad (2)$$

* wanglf@ihep.ac.cn

PRECISION MECHANICS

Nano-positioning
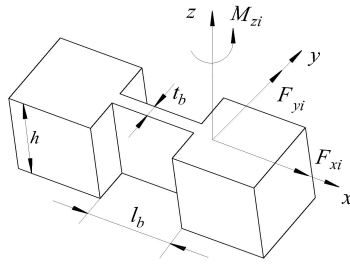
Figure 2: Prismatic beam hinge.

The static analysis of the bridge amplifier mechanism is further conducted. Due to the inherent symmetry and identical parameter sizes of each prismatic beam hinge in the bridge mechanism, only one-quarter of its structure needs to be modeled and analyzed.
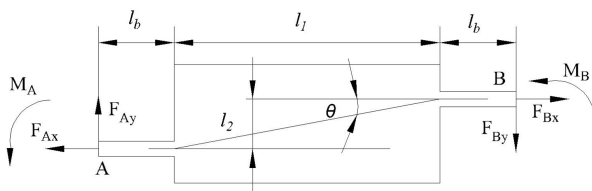
Figure 3: Force condition.

According to the Euler-Bernoulli theory, the torque acting at point A or point B is equivalent, and the stress of the bridge mechanism can be determined based on the stress equilibrium conditions.

$$F_{Ax} = F_{Bx} = F_x = \frac{F_{pzt}}{2} \quad (3)$$

$$F_{Ay} = F_{By} = F_y = \frac{F_s}{2} \quad (4)$$

$$M_A = M_B = M = \frac{F_x l_2 - F_y l_1}{2} \quad (5)$$

In the above equations, F_{pzt} and F_s are respectively the input force and the reaction force of the end load of the bridge mechanism.

The prismatic beam hinge shares identical force conditions and dimensions, experiencing equivalent deformation. By substituting Eqs. (3)-(5) into Eq. (2), its deformation can be calculated.

$$\Delta x = c_{11} F_x w \quad (6)$$

$$\Delta y = c_{22} F_y + c_{23} M \quad (7)$$

$$\Delta \theta = c_{32} F_y + c_{33} M \quad (8)$$

The stress analysis diagram of the bridge mechanism in Fig. 3 reveals that the deformation of a single bridge arm is attributed to the flexible hinge's deformation and the rotation of the bridge arm. The expressions for its input displacement ΔX and output displacement ΔY are as follows:

$$\Delta X = 2\Delta x + l_2 \Delta \theta \quad (9)$$

$$\Delta Y = 2\Delta y + l_1 \Delta \theta \quad (10)$$

The input and output displacements of the bridge mechanism are determined by substituting Eqs. (8)-(10) into the aforementioned equations.

$$\Delta X = (c_{11} + \frac{l_2^2 c_{33}}{4})F_{pzt} + (\frac{l_2 c_{32}}{2} - \frac{l_2 l_1 c_{33}}{4})F_s \quad (11)$$

$$\Delta Y = (\frac{l_2 c_{23}}{2} + \frac{l_1 l_2 c_{33}}{4})F_{pzt} + (c_{22} + \frac{l_1 c_{32}}{2} - \frac{l_1 c_{23}}{2} - \frac{l_1^2 c_{33}}{4})F_s \quad (12)$$

Reformulate the flexibility matrix of the prismatic beam hinge in Eq. (3) and incorporate it into the aforementioned equation, thereby deriving the displacement amplification ratio of the bridge amplifier mechanism.

$$R_a = \frac{9l_2(l_b + l_1)F_{pzt} + (4l_b^2 + 6t_b^2(1 + u) - 9l_1^2)F_s}{3(t_b^2 + 3l_2^2)F_{pzt} + 9l_2(l_b - l_1)F_s}, \quad (13)$$

where u is the Poisson ratio of the material. And when there is no external load or the external load is very small, the displacement amplification ratio of the bridge mechanism can be regarded as a constant R_{a0}:

$$R_{a0} = \frac{3l_2(l_b + l_1)}{t_b^2 + 3l_2^2}. \quad (14)$$

SIMULATED ANALYSIS

The design platform's performance will be further analyzed and the modeling accuracy verified through finite element analysis in this section. The platform structure model and AL7075 material parameters are imported into Workbench.
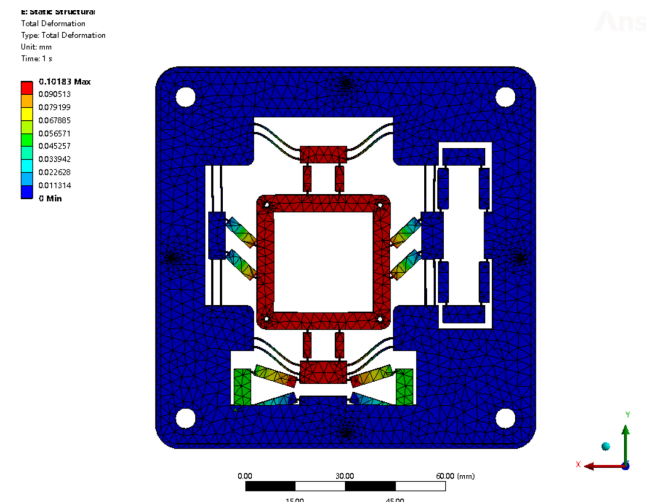
Figure 4: Simulation of displacement amplification ratio.

(a) Y-direction displacement

(b) X-direction displacement
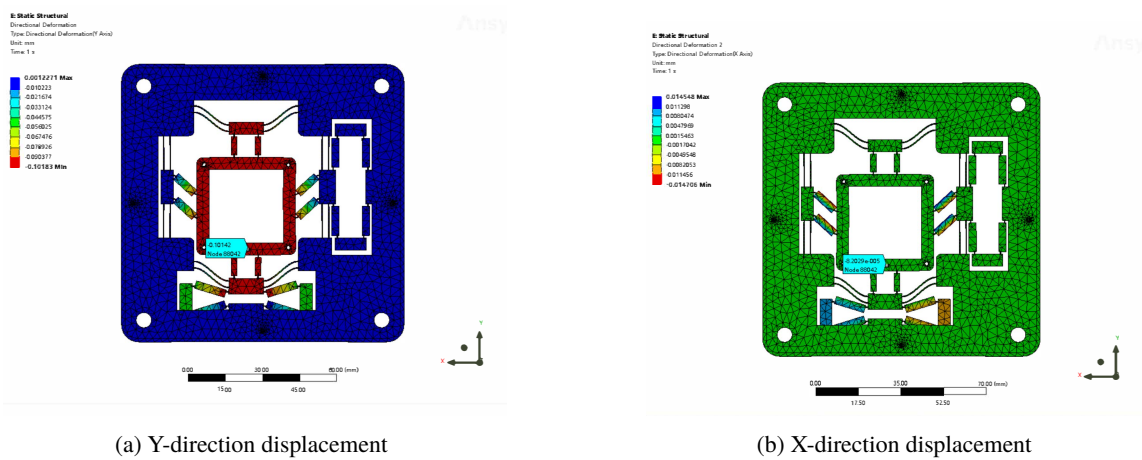
Figure 5: Simulation of platform decoupling characteristics.

(a)

(b)

(c)

(d)

(e)

(f)
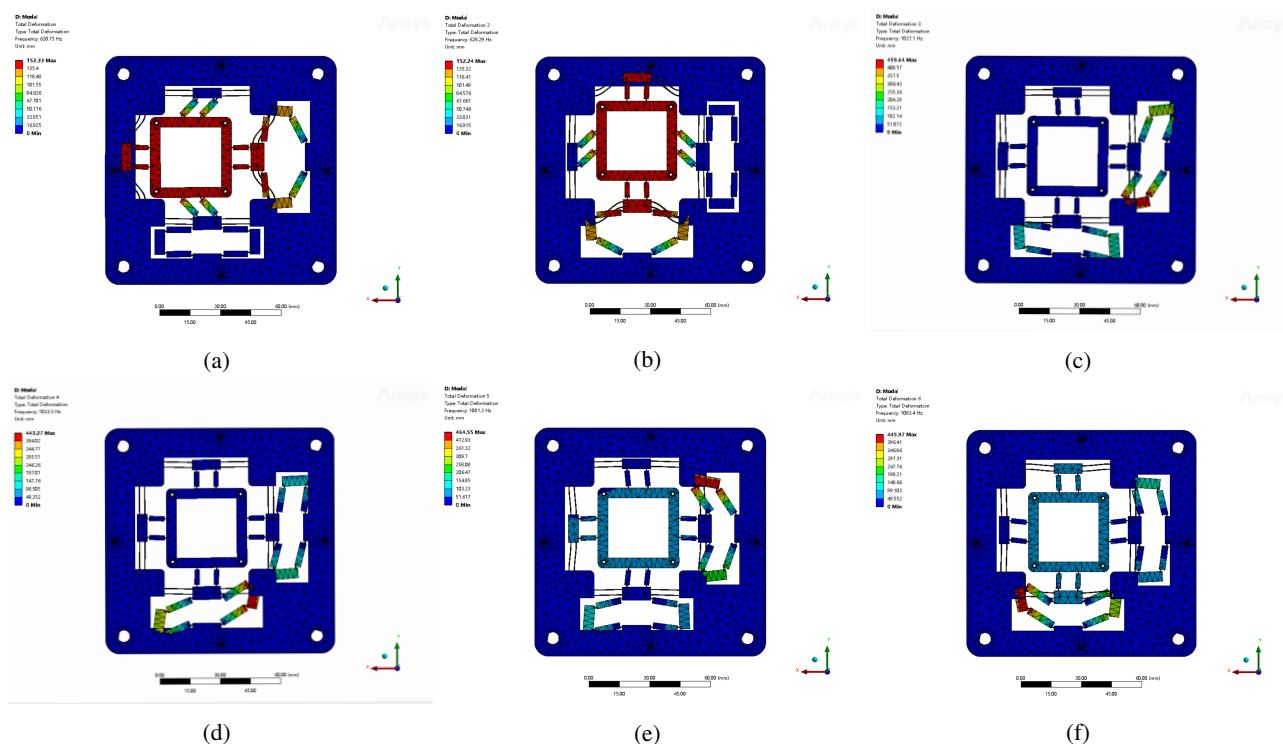
Figure 6: The first six mode shapes of the platform. (a) The first mode, (b) the second mode, (c) the third mode, (d) the fourth mode, (e) the fifth mode, (f) the sixth mode.

Static Simulation

In the static simulation, a fixed constraint is applied to the fixed hole positions at the four corners of the platform. The input displacements of 10 µm are separately applied to both inputs of the bridge amplification mechanism in order to obtain the output displacement of the platform, as depicted in Fig. 4. The simulation results demonstrate that the terminal output displacement of the platform measures 101.42 µm, with a corresponding displacement amplification ratio reaching up to 10.142.

Furthermore, it is imperative to conduct an analysis on the decoupling characteristics of the platform and separately compare its output displacements in the y-direction and x-

direction under the aforementioned conditions, as depicted in Fig. 5. The results reveal that the platform exhibits an output displacement of 101.42 µm in the y-direction, while only 0.08 µm in the x-direction. Consequently, a coupling error of merely 0.07 % is observed, indicating a remarkable decoupling capability possessed by this platform.

Modal Analysis

The modal characteristics of the flexible mechanism significantly influence the dynamic behavior of the entire system and impact the tracking control performance. Therefore, a modal analysis of the platform is conducted in this section. As illustrated in Fig. 6, the first six modes of the platform are presented. Due to the symmetrical structure of the platform,

the modes manifest in pairs. The first six modes correspond to 620.7 Hz, 628.2 Hz, 1027.1 Hz, 1033.3 Hz, 1081.3 Hz, and 1083.4 Hz. Consequently, the platform exhibits remarkable dynamic characteristics.

Stress Analysis

Ensuring a large output displacement while maintaining the stress condition of the platform is crucial. In this section, the maximum stress of the platform is simulated. As illustrated from the simulation results presented in Fig. 7, the maximum stress occurs at the connecting flexible hinge of the inner guiding mechanism of the platform. The maximum stress of the platform is 108.66 MPa, which is significantly lower than the material's yield strength of 455 MPa.
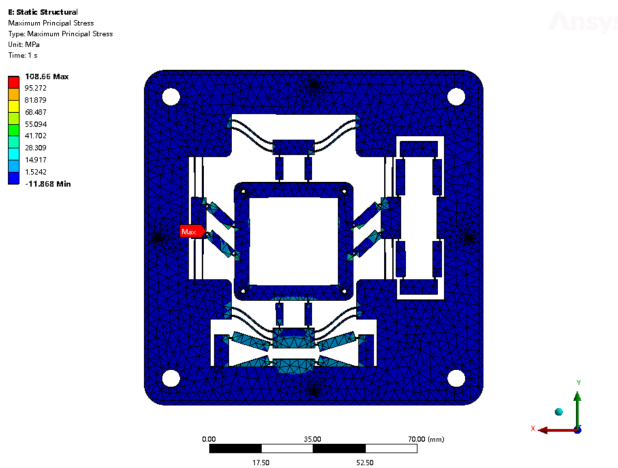
Figure 7: Maximum stress of the platform.

FUTURE WORK

After executing the mechanical design, modeling, and ANSYS simulation of the XY scanning platform, we shall proceed to fabricate the platform, construct a real-time control system with a voltage amplifier and an NI controller, and implement a high-precision, high-dynamic rapid closed-loop control of the platform using a laser interferometer as a sensor.

CONCLUSION

In this paper, we propose an XY piezoelectric scanning platform for synchrotron radiation light source, introduce the structure and composition of the platform, and clarify its working principle. The amplification ratio of the bridge amplifier mechanism is analyzed via the static model, and further validated by finite element simulation. The results indicate that the platform exhibits an amplification ratio surpassing 10. The implementation of two sets of guiding mechanisms enables the platform to exhibit a high degree of decoupling. The overall symmetry and compact structure design of the platform also ensure its excellent dynamic characteristics, with the first-order natural frequency reaching up to 620 Hz.

REFERENCES

[1] E. Nazaretski *et al.*, "Design and performance of an X-ray scanning microscope at the Hard X-ray Nanoprobe beamline of NSLS-II", *J. Synchrotron Radiat.*, vol. 24, no. 6, pp. 1113-1119, 2017. doi:10.1107/S1600577517011183

[2] X. Chen *et al.*, "Quantitative microstructural imaging by scanning Laue x-ray micro-and nanodiffraction", *MRS Bulletin*, vol. 41, no. 6, pp. 445-453, 2016. doi:10.1557/mrs.2016.97

[3] C.G. Schroer *et al.*, "Hard X-ray nanoprobe at beamline P06 at PETRA III", *Nucl. Instrum. Methods Phys. Res., Sect. A*, vol. 616, no. 2-3, pp. 93-97, 2010. doi:10.1016/j.nima.2009.10.094

[4] J.J. Deng *et al.*, "The velociprobe: An ultrafast hard x-ray nanoprobe for high-resolution ptychographic imaging", *Rev. Sci. Instrum.*, vol. 90, no. 8, p. 083701, 2019. doi:10.1063/1.5103173

[5] G. Martínez-Criado *et al.*, "ID16B: a hard X-ray nanoprobe beamline at the ESRF for nano-analysis", *J. Synchrotron Radiat.*, vol. 23, no. 1, pp. 344-352, 2016. doi:10.1107/S1600577515019839

[6] Y. Koseki *et al.*, "Kinematic analysis of a translational 3-d.o.f. micro-parallel mechanism using the matrix method", *Adv. Rob.*, vol. 16, no. 3, pp. 251-264, 2002. doi:10.1163/156855302760121927